Nanoscale

Accepted Manuscript

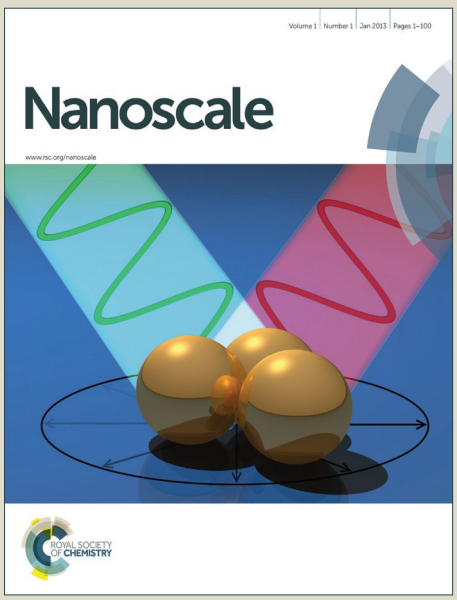

ROYAL SOCIETY OF CHEMISTRY

www.rsc.org/nanoscale

Nanoscale

ARTICLE

Nondestructive Optical Visualisation of Graphene Domains and Boundaries

Xingyi Wu, Guofang Zhong* and John Robertson

Received 00th January 20xx,
Accepted 00th January 20xx

DOI: 10.1039/x0xx00000x

www.rsc.org/nanoscale

Domain boundaries of polycrystalline graphene produced by chemical vapor deposition (CVD) adversely influence the graphene transporting properties. Existing domain visualisation methods for large area graphene always cause detrimental damage or contamination. Here we report a nondestructive method for spatial visualisation of the domains and boundaries of large area continuous graphene grown on Cu foils (Gr/Cu) by CVD. Using a rationally modified optical microscope, we can directly observe novel star-like bright line sets of Gr/Cu under an enhanced dark field mode. Each set of the bright lines are identified as the ridges of one Cu surface pyramid which arises beneath one enlarging graphene domain due to slower evaporation of graphene-covered Cu than that of graphene-free Cu. This one to one correspondence thereby enables the nondestructive visualisation. This method offers an advantageous pathway for monitoring the spatial distribution of the graphene domains and boundaries. We have further discovered for the first time various types of star-like ridge structures which are governed by the underlying Cu crystallographic orientations. This raises new phenomenon for research on the complex 2D material-metal interfacing.

Introduction

Large area, high quality, continuous monolayer graphene films are indispensable matrix for industrial manufacture of graphene-based high-end devices.[1–3] Among various synthesis methods, Cu-catalyzed chemical vapor deposition (Cu-CVD) stands out as the most promising for industrial production of graphene because it simultaneously fulfills industrial demands for high quality, monolayer uniformity, process scalability, and film continuity.[4] However, continuous graphene films grown by Cu-CVD are always polycrystalline.[5,6] The boundaries unavoidably emerge from the coalescence of nearby graphene domains.[7] (Hereafter, "grain" and "domain" are used for polycrystalline Cu metal and graphene films, respectively.) The boundaries influence the transporting properties of graphene and consequently alter the performances of graphene-based devices,[8–10] which further causes detrimental inhomogeneity to the entire manufactured device arrays. Recently, progresses have been made to drastically reduce the density of boundaries by increasing the domain sizes via modified Cu-CVD technologies.[11–14] The largest domains at present have reached centimeter scale.[13] On the other hand, the boundary-associated adverse effects can be efficiently controlled by spatial visualisation of the domains and boundaries. A potential visualisation procedure can mark the boundary-infected devices under the navigation of the mapped domains and boundaries of the post-growth graphene films. The boundary-limited products yield can then be evaluated and the quality reliability determined. In this sense, an effective visualisation method is extraordinarily valuable for manufacture management of CVD graphene-based devices.

The graphene domain boundaries can be detected by atomic resolution microscopes such as TEM[5,6]or STM[15,16] and spectroscopic mappings such as Raman.[17,18] These methods are non-invasive with high accuracy but limited to much smaller scale than industry demanded. In recent years, scalable visualisation approaches have been developed, many of which can be approximately classified into two major types. The first type is to selectively decorate the graphene domain boundaries using specific chemical species due to the relatively high reactivity of the boundaries. The decorated boundaries can be readily distinguished from the rest graphene surfaces by microscopes. Conventionally used decorating groups include oxidants such as radicalized oxygen[19] or permanganate[20] and metals such as gold nanoparticles.[21] The other is to visualise the graphene domains by mapping the graphene orientation-dependent alignment of the "quasi-epitaxial" coatings. For

Department of Engineering, University of Cambridge, Cambridge CB3 0FA, UK.
E-mail: gz222@cam.ac.uk

†Electronic Supplementary Information (ESI) available: Photograph of alternative EDF-OM setup, schematic optical configurations of the EDF-OM and BF-OM, high magnification SEM images of the ridge structure, EDF-OM images of additional types of ridge structures, supplementary movies recording the evolution from BF-OM images to EDF-OM images of both the discontinuous and continuous Gr/Cu samples. See DOI: 10.1039/x0xx00000x

instance, nematic liquid crystals coated on graphene surfaces assemble along specific directions corresponding to the underlying graphene domain orientations.[22,23] Similar direction correspondence also exists between the graphene-supported MoS_2 flakes grown by CVD and the underlying graphene.[24] However, these methods are destructive to graphene since they have to either partially damage carbon bonds or induce contaminating coatings or transfer graphene onto secondary substrates. Therefore, a nondestructive and scalable visualisation technique is urgently desired but currently lacking. In principle, if an ideal visualisation method is to nondestructively map the graphene domains and boundaries, it should preferably detect certain intrinsic characteristics of graphene rather than any derivative physical or chemical effects induced by external interferences. Moreover, the potential 'intrinsic characteristics' should also be spatially specific to individual graphene domains so as to distinguish the geometric locations of the inter-connected domains. Based on this analysis and latest experimental findings, we have rationally designed a novel optical method, which, for the first time, can nondestructively visualise the domains and boundaries of large area continuous graphene films grown on polycrystalline Cu foils (Gr/Cu) by CVD.

Results and discussion

Our design is inspired by recent discoveries of the dynamic formation of Cu surface pyramids during the Cu-catalyzed CVD graphene growth.[25–27] The schematic drawing in Fig. 1a illustrates this process. Basically, there is a pre-melted surface Cu layer at the typical graphene growth temperature of ~1000°C (the melting temperature T_m of bulk Cu is 1083°C in ambient conditions). The pre-melted Cu atoms are evaporated substantially and removed by the CVD carrier gas,[28] which has a higher rate in graphene-free regions than in graphene-covered regions.[29,30] Therefore, the Cu surface outside an enlarging graphene domain loses Cu atoms much faster than that below the domain. In the case of a hexagonal graphene domain, the Cu surface below the domain, which is originally flat, will accordingly evolve into a hexagonal pyramid via the lateral evaporation (Fig. 1a).[27] Here we point out that, if viewed from the perpendicular direction, the hexagonal pyramid will appear as a star-like ridge set. If the fingerprint ridge sets can be visualised in some route, the spatial distribution of graphene domains and boundaries can be straightforward determined. Since the ridges are intrinsic features of the graphene-Cu interfacial morphology, the potential visualisation process could be nondestructive.

In this study, we demonstrate that the star-like ridge sets of Gr/Cu can be clearly imaged by a modified optical microscope (OM) under an enhanced dark field mode (EDF). Fig. 2a shows the setup of our EDF-OM which is developed from an upright OM. We only use an external illumination light source such as an annular tube or a desk lamp instead of its original internal light source, as shown in Fig. 2a and Fig. S1, respectively (see Experimental for more details). The EDF-OM is then used to image discontinuous graphene samples which have been grown on commercial polycrystalline Cu foils via CH_4 decomposition using an atmospheric pressure CVD recipe reported recently.[31] Fig. 2b shows one of the EDF-OM images of isolated hexagonal graphene domains. A star-like ridge set is clearly revealed which radially diverges from the domain center straightforward to the domain vertices. The entire structure is morphologically identical to the schematic in Fig. 1, i.e., each set of ridges exactly follows the diagonals of each graphene domain since the Cu surface pyramid inherits the geometric symmetry of the domain. This one to one correspondence, as will be shown, thereby enables nondestructive visualisation of the domains and boundaries of continuous graphene. In addition, feather-like features along some of the ridges are also observed, which make the entire domain much brighter than the surrounding Cu background.

Since the as-grown Gr/Cu sample is invisible under bright-field OM (BF-OM), the sample is mildly oxidized in air to enable BF-OM observation of the isolated domain.[32] Fig. 2c displays a BF-OM image of the same domain obtained after mild oxidation. It only shows homogenous optical contrast inside the domain, providing no clues for any star-like ridges. The enormous difference between the EDF-OM and BF-OM observations is further demonstrated in Supplementary Movie 1, which records the real time evolution from Fig. 2c to Fig. 2b under constant external light intensity and decreasing internal light intensity (from max to zero). Such a difference originates from their different optical configurations. The external light source of the EDF-OM provides large-angle oblique incident light (~50° relative to the sample plane, see Fig. 2a and Fig. S2a), while the internal BF light source gives almost vertical incident light with a much smaller incident angle (Fig. S2b). Under EDF-OM, most of the oblique incident light from the external light source will be specularly reflected away from the objective by any smooth surfaces. However, as the star-like ridges experience significant curvature changes between adjacent pyramid faces, they are much rougher than the faces and thereby could scatter much more light into the objective (see Fig. S2a). Therefore, the ridges are visualised as star-like bright line sets. On the contrary, under BF-OM, most of the vertical internal incident light will be reflected back into the objective, which results in no visible contrast between the ridges and the faces (see Fig. S2b). We find that a pristine DF-OM using the hollow cone-shaped internal light can also visualise the star-like ridges, but the resulted contrast is too low and the brightness too weak, which might account for its neglect in previous research.[33] This is probably because of the small incident angle and the weak intensity of the internal DF light. We regard our novel setup as the EDF-OM also because of the external source-enhanced incident angle and light intensity.

Similar to the BF-OM, the low magnification SEM image of the same domain (Fig. 2d) barely shows any ridge-like features. This agrees with previous SEM investigations reporting homogeneous optical contrast inside the Cu-catalyzed graphene domains.[7] However, close observations under high magnifications along the domain diagonals strongly indicate the existence of the star-like ridges, as shown in Fig. 2e and Fig. S3, which appear slightly brighter than the surrounding domain

background. This thereby supports the EDF-OM discovery of the star-like ridge set. It should be noted that this is the first time that such a ridge structure is formally manifested by SEM. However, although SEM can capture an intrinsically identical ridge structure as the EDF-OM, it only generates much lower contrast than the EDF-OM. Thereby the EDF-OM is much more advantageous than the high magnification SEM in imaging the graphene ridge structures for visualisation of large scale graphene domains and boundaries.

In addition to the well-defined star-like six-ridge structure that has been shown above, we have further discovered, for the first time, a plethora of novel star-like ridge sets which do not always exhibit six ridges, as summarized in Fig. 3a-f and Fig. S4. These structures differ from each other. Most remarkably, the structures in Fig. 3a-e have visible ridges while that in Fig. 3f has no observable ridges at all.

We have further found that the morphologies of the various star-like ridge sets are governed by the underlying Cu crystallographic orientations. Fig. 3g shows an EDF-OM image of multiple types of star-like ridge sets formed on a polycrystalline Cu region, while Fig. 3h shows the crystallographic orientation map of the underlying Cu grains characterised by the electron backscattering diffraction (EBSD). The Miller indexes of the Cu grains are also marked inside Fig. 3a-f and also illustrated by their outline colours with reference to the colour key inset in Fig. 3h. It can be clearly seen that different types of star-like ridge sets are formed on different Cu grains while those on the same Cu grain are of exactly the same type. In particular, one graphene domain grown over multiple Cu grains, as seen in Fig. 3c, has mixed types of ridges in accordance with the crystallographic orientations of the respective Cu grains. It should be noted that this is the first time that these diverse Cu crystallographic orientation-dependent star-like ridge sets are discovered, although there has been intense research on polycrystalline Cu-catalyzed graphene growth and its characterisation.[34] This is most likely because their morphological differences can be hardly observed under the commonly used BF-OM and SEM. Although the three dimensional laser microscopy has found a ridge structure resembling that in Fig. 3a,[26] no other types of the star-like ridge sets have been reported. The various star-like ridge structures thereby raise new phenomenon for fundamental graphene research beyond the current scope.

As the visibility of the ridge structure is determined by the curvature change between the adjacent pyramid faces, smaller dihedral angle β (Fig. 1b) should enhance the ridge visibility. For simplicity, considering the case of a hexagonal Cu pyramid as illustrated in Fig. 1b, β can be calculated as:

$$\sin\frac{\beta}{2}=\sqrt{\frac{1+\left(\frac{h}{a}\right)^2}{1+\frac{4}{3}\cdot\left(\frac{h}{a}\right)^2}}\approx 1-\frac{1}{6}\cdot\left(\frac{h}{a}\right)^2,(h<<a) \qquad (1)$$

where h is the height of the pyramid and a is the lateral length of the hexagonal graphene domain. Assuming that both the lateral growth rate of graphene γ_{gr}, and the evaporation rate of graphene-free Cu γ_{Cu}, are constant, Eq. 1 can be further approximated by:

$$\sin\frac{\beta}{2}\approx 1-\frac{1}{6}\cdot\left(\frac{\gamma_{Cu}}{\gamma_{gr}}\right)^2. \qquad (2)$$

Here, γ_{Cu} depends on the CVD processing temperature T, the standard vapor pressure of Cu P_{cu} and total ambient pressure P,[35] while γ_{gr} can be taken proportional to the partial pressure of hydrocarbon gas P_C in a first-order reaction:

$$\gamma_{Cu}=\frac{P_{Cu}-P}{\sqrt{2\pi MRT}}, \qquad (3)$$

$$\gamma_{gr}=k\cdot P_C, \qquad (4)$$

where M is the molecular weight of Cu, R is the universal gas constant, and k is the first-order graphene growth rate constant. Eq. 2-4 relate the ridge visibility to the CVD graphene growth kinetics. The conditions using high processing temperature (~1000 °C) and low hydrocarbon concentration for synthesis of high quality graphene favor the formation of observable ridge structures.[36,37] Considering that atmospheric pressure is used throughout our CVD processes, graphene grown by the most commonly used low pressure CVD (~1Torr) should have more pronounced ridges due to faster Cu evaporation.[37] In addition, it should be noted that the visibility of the ridge structures is also influenced by the crystallographic orientations of the Cu grains as previously shown in Fig. 3. During CVD processes, high temperature annealing promotes formation of large Cu grains with low-energy crystallographic surfaces, mostly (110), (100) and (111) (The absence of these exact low-index surfaces from our EBSD results is probably due to the deformation of the Cu foils during sample handling). It has been well established that the thermal stability of the low-index fcc metal surface follows its in-plane packing density. Generally the relatively open (110) and (100) surfaces start to disorder and pre-melt at temperature below T_m while the most densely packed (111) surface keeps in a crystalline state up to T_m and shows weak superheating effects.[38,39] This can qualitatively explain our observations in Fig. 3. Since a lower stability results in a higher evaporation rate of Cu, the visibility of the ridge structures under EDF-OM varies on different Cu crystallographic surfaces. As the (111) surface is of the highest stability, the ridge structures can hardly form on (111)-vicinal Cu surfaces under our CVD conditions, therefore the graphene domains on (111)-vicinal Cu surfaces are barely visible under EDF-OM (see Fig. 3f). However, most of the graphene domains grown on other Cu grains are more or less visible because of their relatively lower surface stability (see Fig. 3a-e). As for the additional features making parts of the graphene domains brighter, particularly noticeable in Fig. 3b and 3e, their formation probably lies in the reconstruction of the Cu surfaces under the template effect of graphene domains during both the isothermal growth and cooling processes.[27,40] This is essential since the graphene-covered Cu pyramid faces are usually in higher energy states

compared to the low-energy surfaces of the graphene-free Cu grains formed during annealing. The reconstruction will transform the atomic flat pre-melted Cu surfaces into 'step-wise rough' facets,[27] some of which might be rough enough to be visualised by the EDF-OM. The reconstruction also varies depending on the crystallographic properties of the Cu grains.[27,40] It should also be noted that if the graphene growth rate is so high as to rapidly form continuous graphene, or the growth temperature is too low which suppresses the evaporation of Cu, the ridge structures can hardly form on Cu and thereby the graphene domains might be barely visible under the EDF-OM.

At this point we have confirmed that the star-like ridge structures arise from the intrinsic morphologies of graphene-Cu interfacing and can be clearly imaged by the EDF-OM. We now demonstrate the non-destructive visualisation of the star-like ridge structures of continuous Gr/Cu and its application in outlining the domain boundaries and estimating the domain density. Fig. 4a-c show three typical images, taken by EDF-OM, BF-OM and SEM, respectively, of the same continuous Gr/Cu sample. The EDF-OM image in Fig. 4a clearly exhibits multiple sets of star-like ridges. In contrast, the BF-OM and SEM images in Fig. 4b and 4c merely show the Cu surface morphology with a uniform colour contrast. As each set of star-like ridges spatially tags one graphene domain, we can use the ridge intersection to mark the nucleation center of each domain and the ridge endpoints to delineate the neighboring domains. Fig. 4d shows the same EDF-OM image as Fig. 4a with individual domains approximately outlined by the yellow polygons based on their corresponding star-like ridges. The graphene nucleation centers (ridge intersections) are generally deviated away from the geometrical centers of the domains as a consequence of the competitive growth of the neighboring domains.[27] The domain density in Fig. 4d is counted to be ~5.5 mm^{-2} and thus the average domain size is ~0.18 mm^{-2}. Fig. 4e and 4f further illustrate the EDF-OM images of continuous graphene grown on other Cu grains under the same CVD conditions with their domains outlined by the yellow polygons. It should be noted that our optical visualisation approach works only under the EDF-OM mode. This is further demonstrated in Supplementary Movie 2 which records the evolution of from Fig. 4b to Fig. 4a with constant external light intensity and decreasing internal light intensity.

Since the graphene domain density saturates with increasing coverage during Cu-CVD growth,[41] we substantiate the reliability of our visualisation method by comparing the domain density and size distribution visualised at full coverage to those counted at partial coverage. Fig. 4g plots the graphene domain density against the corresponding coverage. The coverage is measured from both the EDF-OM and BF-OM images, but the Gr/Cu sample is mildly oxidized for BF-OM observations. The domain density up to ~30% coverage can be accurately counted from the BF-OM image since most domains are spatially isolated. However, the BF-OM method begins to cause noticeable errors after ~60% coverage and completely fails at >80% coverage as an increasing number of domains are becoming inter-connected. In contrast, the EDF-OM approach can figure out the domain density from zero up to full coverage. We can see from Fig. 4g that the domain density at full coverage, which can be visualized only by the EDF-OM, has limited discrepancy (~14%) with the domain density at lower coverages (~30% and ~60%), which can be counted by both the EDF-OM and the BF-OM. Fig. 4h shows that the domain size distribution at full coverage (determined by EDF-OM) is also in consistence with that at partial coverage (determined by both EDF-OM and BF-OM). Fig. 4i shows that there is no significant discrimination for the domain densities of discontinuous graphene counted from crystallographically different Cu grains. This agrees with previous results at similar growth temperature.[42] These observations justify that our EDF-OM visualisation method is effective and reliable for continuous graphene films although the ridge structure of the domains grown on (111)-vicinal Cu grains are less visible than the rest.

We highlight that our visualisation method has significant advantages over the up-to-date methods. First of all, it is nondestructive since we directly observe the Gr/Cu samples by an optical microscope with no need for oxidation, assistive coatings or transfer. Moreover, it is scalable, cost-saving, and rapid because an optical microscope works in ambient conditions by frame-to-frame scan.

Conclusions

In summary, we have developed a novel EDF-OM method for visualising the domains and boundaries of large are continuous Gr/Cu. It is based on a variety of novel star-like ridge sets which are formed during CVD growth as inherent morphologies of the graphene-Cu interfaces The ridge structure-enabled visualisation approach is purely optical and thereby, for the first time, not only completely nondestructive to graphene but also applicable to large area samples. Therefore, this research opens a new route towards nondestructively assessing and controlling the boundary-associated adverse effects on the graphene-based devices that are manufactured in the industry scale. Furthermore, we find that the morphologies of the various types of ridge sets vary depending on the underlying Cu crystallographic orientations. This is a new phenomenon beyond current knowledge of polycrystalline metal-catalyzed graphene growth. It strongly indicates the complexity of graphene-Cu thermodynamic interactions for which a comprehensive understanding should take into account the thermal stability of the Cu facets.

Experimental

Graphene synthesis

Graphene is grown on Cu foils using atmospheric pressure CVD.[31] Electropolished Cu foils (Alfa Aesar, 25 μm thickness, 99.8% purity) are used as catalysts. Ramping and annealing is carried out in Ar atmosphere (490 sccm) at 1030 °C (total pressure ~ 1 bar, heating rate ~ 40 °C /min). In a benchmark one-step CVD process, CH_4 (~0.12 sccm) and H_2 (10 sccm) are then added to the Ar gas followed by cooling in Ar and H_2. It takes

~95 min to grow continuous monolayer graphene films. Isolated graphene domains are obtained by terminating the CH_4 supply before the domains merge.

Characterisation

The Gr/Cu samples are characterised by optical microscope (Nikon ECLIPSE LV150N) in both the EDF and the BF modes, SEM (Zeiss SIGMA VP) and EBSD (Oxford NordlysMax EBSD detector mounted on Philips XL30 sFEG SEM). For the EDF-OM observations, an external illumination light source such as an annular light tube or a desk lamp is used instead of its original internal light source. To record the supplementary movies, the external light source is kept on constant intensity while the internal light intensity is manually decreased from the maximum intensity to zero. For the BF-OM observations of isolated graphene domains, the pristine Gr/Cu samples are mildly oxidized in air at 200 °C for 1 min.[32]

Acknowledgements

The authors acknowledge funding from the EC project GRAFOL, CP-IP 285275. They thank Girish Rughoobur from Cambridge University Engineering Department for help with the three dimensional schematic drawings. They also thank Prof. Stephan Hofmann from Cambridge University Engineering Department and his group members for helpful discussions of this work. X.W. acknowledges funding from St. John's College, University of Cambridge, and scholarships from the Cambridge Overseas Trust.

References

1 K. S. Novoselov, A. K. Geim, S. V. Morozov, D. Jiang, Y. Zhang, S. V. Dubonos, I. V. Grigorieva and A. A. Firsov, *Science*, 2004, **306**, 666–669.
2 A. K. Geim, *Science*, 2009, **324**, 1530–1534.
3 K. S. Novoselov, V. I. Fal'ko, L. Colombo, P. R. Gellert, M. G. Schwab and K. Kim, *Nature*, 2012, **490**, 192–200.
4 S. Hofmann, P. Braeuninger-Weimer and R. S. Weatherup, *J. Phys. Chem. Lett.*, 2015, **6**, 2714–2721.
5 P. Y. Huang, C. S. Ruiz-Vargas, A. M. van der Zande, W. S. Whitney, M. P. Levendorf, J. W. Kevek, S. Garg, J. S. Alden, C. J. Hustedt, Y. Zhu, J. Park, P. L. McEuen and D. A. Muller, *Nature*, 2011, **469**, 389–392.
6 K. Kim, Z. Lee, W. Regan, C. Kisielowski, M. F. Crommie and A. Zettl, *ACS Nano*, 2011, **5**, 2142–2146.
7 X. Li, W. Cai, J. An, S. Kim, J. Nah, D. Yang, R. Piner, A. Velamakanni, I. Jung, E. Tutuc, S. K. Banerjee, L. Colombo and R. S. Ruoff, *Science*, 2009, **324**, 1312–1314.
8 O. V. Yazyev and S. G. Louie, *Nat. Mater.*, 2010, **9**, 806–809.
9 O. V. Yazyev and S. G. Louie, *Phys. Rev. B*, 2010, **81**, 195420.
10 L. A. Jauregui, H. Cao, W. Wu, Q. Yu and Y. P. Chen, *Solid State Commun.*, 2011, **151**, 1100–1104.
11 Z. Yan, J. Lin, Z. Peng, Z. Sun, Y. Zhu, L. Li, C. Xiang, E. L. Samuel, C. Kittrell and J. M. Tour, *ACS Nano*, 2012, **6**, 9110–9117.
12 H. Zhou, W. J. Yu, L. Liu, R. Cheng, Y. Chen, X. Huang, Y. Liu, Y. Wang, Y. Huang and X. Duan, *Nat. Commun.*, 2013, **4**, 2096.
13 Y. Hao, M. S. Bharathi, L. Wang, Y. Liu, H. Chen, S. Nie, X. Wang, H. Chou, C. Tan, B. Fallahazad, H. Ramanarayan, C. W. Magnuson, E. Tutuc, B. I. Yakobson, K. F. McCarty, Y.-W. Zhang, P. Kim, J. Hone, L. Colombo and R. S. Ruoff, *Science*, 2013, **342**, 720–723.
14 A. Mohsin, L. Liu, P. Liu, W. Deng, I. N. Ivanov, G. Li, O. E. Dyck, G. Duscher, J. R. Dunlap, K. Xiao and G. Gu, *ACS Nano*, 2013, **7**, 8924–8931.
15 K. W. Clark, X.-G. Zhang, I. V. Vlassiouk, G. He, R. M. Feenstra and A.-P. Li, *ACS Nano*, 2013, **7**, 7956–7966.
16 L. Gao, J. R. Guest and N. P. Guisinger, *Nano Lett.*, 2010, **10**, 3512–3516.
17 Q. Yu, L. A. Jauregui, W. Wu, R. Colby, J. Tian, Z. Su, H. Cao, Z. Liu, D. Pandey, D. Wei, T. F. Chung, P. Peng, N. P. Guisinger, E. A. Stach, J. Bao, S.-S. Pei and Y. P. Chen, *Nat. Mater.*, 2011, **10**, 443–449.
18 S. Wang, S. Suzuki and H. Hibino, *Nanoscale*, 2014, **6**, 13838–13844.
19 D. L. Duong, G. H. Han, S. M. Lee, F. Gunes, E. S. Kim, S. T. Kim, H. Kim, Q. H. Ta, K. P. So, S. J. Yoon, S. J. Chae, Y. W. Jo, M. H. Park, S. H. Chae, S. C. Lim, J. Y. Choi and Y. H. Lee, *Nature*, 2012, **490**, 235–239.
20 S. U. Yu, Y. Cho, B. Park, N. Kim, I. S. Youn, M. Son, J. K. Kim, H. C. Choi and K. S. Kim, *Chem. Commun.*, 2013, **49**, 5474.
21 S. U. Yu, B. Park, Y. Cho, S. Hyun, J. K. Kim and K. S. Kim, *ACS Nano*, 2014, **8**, 8662–8668.
22 D. W. Kim, Y. H. Kim, H. S. Jeong and H.-T. Jung, *Nat. Nanotechnol.*, 2012, **7**, 29–34.
23 J.-H. Son, S.-J. Baeck, M.-H. Park, J.-B. Lee, C.-W. Yang, J.-K. Song, W.-C. Zin and J.-H. Ahn, *Nat. Commun.*, 2014, **5**, 3484.
24 H. Ago, S. Fukamachi, H. Endo, P. Solís-Fernández, R. Mohamad Yunus, Y. Uchida, V. Panchal, O. Kazakova and M. Tsuji, *ACS Nano*, 2016, **10**, 3233–3240.
25 J. M. Wofford, S. Nie, K. F. McCarty, N. C. Bartelt and O. D. Dubon, *Nano Lett.*, 2010, **10**, 4890–4896.
26 S. Zhu, Q. Li, Q. Chen, W. Liu, X. Li, J. Zhang, Q. Wang, X. Wang and H. Liu, *RSC Adv.*, 2014, **4**, 32941.
27 Z.-J. Wang, G. Weinberg, Q. Zhang, T. Lunkenbein, A. Klein-Hoffmann, M. Kurnatowska, M. Plodinec, Q. Li, L. Chi, R. Schloegl and M.-G. Willinger, *ACS Nano*, 2015, **9**, 1506–1519.
28 S. Chen, H. Ji, H. Chou, Q. Li, H. Li, J. W. Suk, R. Piner, L. Liao, W. Cai and R. S. Ruoff, *Adv. Mater.*, 2013, **25**, 2062–2065.
29 J. S. Bunch, S. S. Verbridge, J. S. Alden, A. M. van der Zande, J. M. Parpia, H. G. Craighead and P. L. McEuen, *Nano Lett.*, 2008, **8**, 2458–2462.
30 N. S. Mueller, A. J. Morfa, D. Abou-Ras, V. Oddone, T. Ciuk and M. Giersig, *Carbon*, 2014, **78**, 347–355.
31 X. Wu, G. Zhong, L. D'Arsié, H. Sugime, S. Esconjauregui, A. W. Robertson and J. Robertson, *Sci. Rep.*, 2016, **6**, 21152.
32 C. Jia, J. Jiang, L. Gan and X. Guo, *Sci. Rep.*, 2012, **2**, 707.
33 X. H. Kong, H. X. Ji, R. D. Piner, H. F. Li, C. W. Magnuson, C. Tan, A. Ismach, H. Chou and R. S. Ruoff, *Appl. Phys. Lett.*, 2013, **103**, 43119.
34 J. D. Wood, S. W. Schmucker, A. S. Lyons, E. Pop and J. W. Lyding, *Nano Lett.*, 2011, **11**, 4547–4554.
35 J. Safarian and T. A. Engh, *Metall. Mater. Trans. A*, 2013, **44**, 747–753.
36 P. R. Kidambi, C. Ducati, B. Dlubak, D. Gardiner, R. S. Weatherup, M.-B. Martin, P. Seneor, H. Coles and S. Hofmann, *J. Phys. Chem. C*, 2012, **116**, 22492–22501.
37 R. Muñoz and C. Gómez-Aleixandre, *Chem. Vap. Depos.*, 2013, **19**, 297–322.

38 B. Chatterjee, *Nature*, 1978, **275**, 203–203.
39 H. Häkkinen and M. Manninen, *Phys. Rev. B*, 1992, **46**, 1725.
40 K. Hayashi, S. Sato and N. Yokoyama, *Nanotechnology*, 2013, **24**, 25603.
41 T. Terasawa and K. Saiki, *Nat. Commun.*, 2015, **6**, 6834.
42 I. Vlassiouk, S. Smirnov, M. Regmi, S. P. Surwade, N. Srivastava, R. Feenstra, G. Eres, C. Parish, N. Lavrik, P. Datskos, S. Dai and P. Fulvio, *J. Phys. Chem. C*, 2013, **117**, 18919–18926.

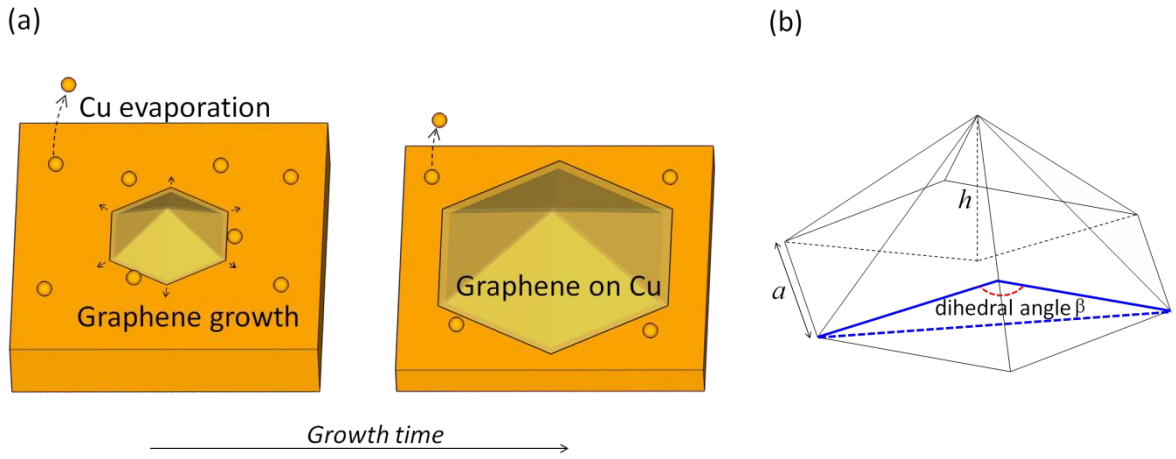

Fig. 1 (a) Schematic illustration of the formation of a Cu surface pyramid under the template effect of an enlarging graphene domain due to the different evaporation rates of Cu between the graphene-covered and graphene-free areas. (b) Sketch of the hexagonal pyramid for calculation of the dihedral angle, where *h* is the height of the pyramid and *a* is the lateral length.

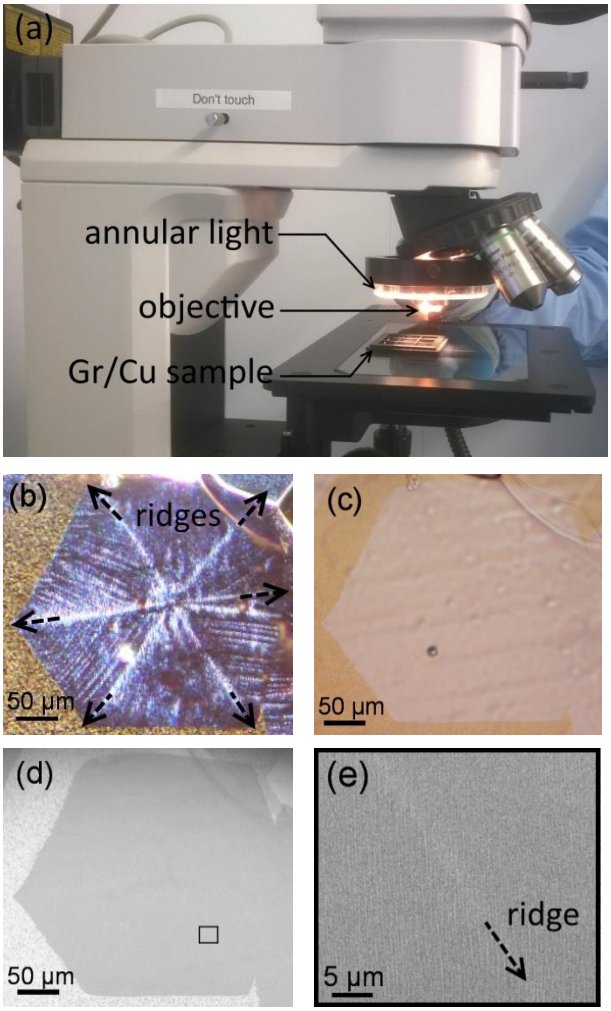

Fig. 2 (a) Setup of the EDF-OM using an external annular light source instead of its original internal light source. (b) EDF-OM, (c) BF-OM and (d) SEM images of the same isolated hexagonal graphene domain grown on Cu. The Gr/Cu sample has been mildly oxidized for BF-OM observation. A set of star-like ridges is observable only by the EDF-OM. (e) High magnification SEM image around a midpoint along one of the domain diagonals marked by the black open box in (d). The black dashed arrow indicates the location and orientation of the ridge.

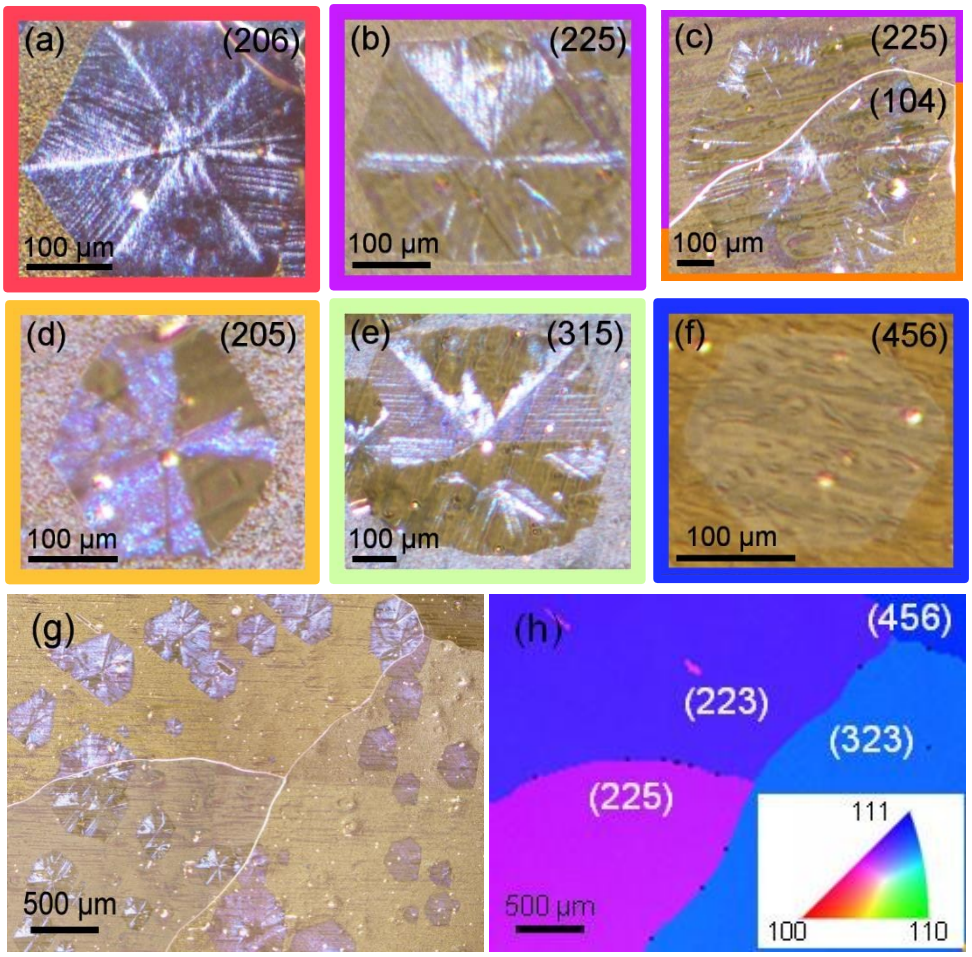

Fig. 3 (a)-(f) EDF-OM images of multi-types of star-like ridges with EBSD-determined Miller indexes of the underlying Cu grains marked inside each panel. The outline colours are set equal to the corresponding EBSD mapping colours of the respective Cu surfaces. The mix-coloured outline of (c) indicates the presence of two different Cu grains below one graphene domain. (g) EDF-OM image of the graphene domains with multi-types of star-like ridges grown over a polycrystalline Cu region. (h) Surface normal-projected inverse pole figure EBSD map of the same region as in (g) with the colour key inset. The sample is tilted at 70° for EBSD scanning and the determined Miller indexes are marked inside each Cu grain.

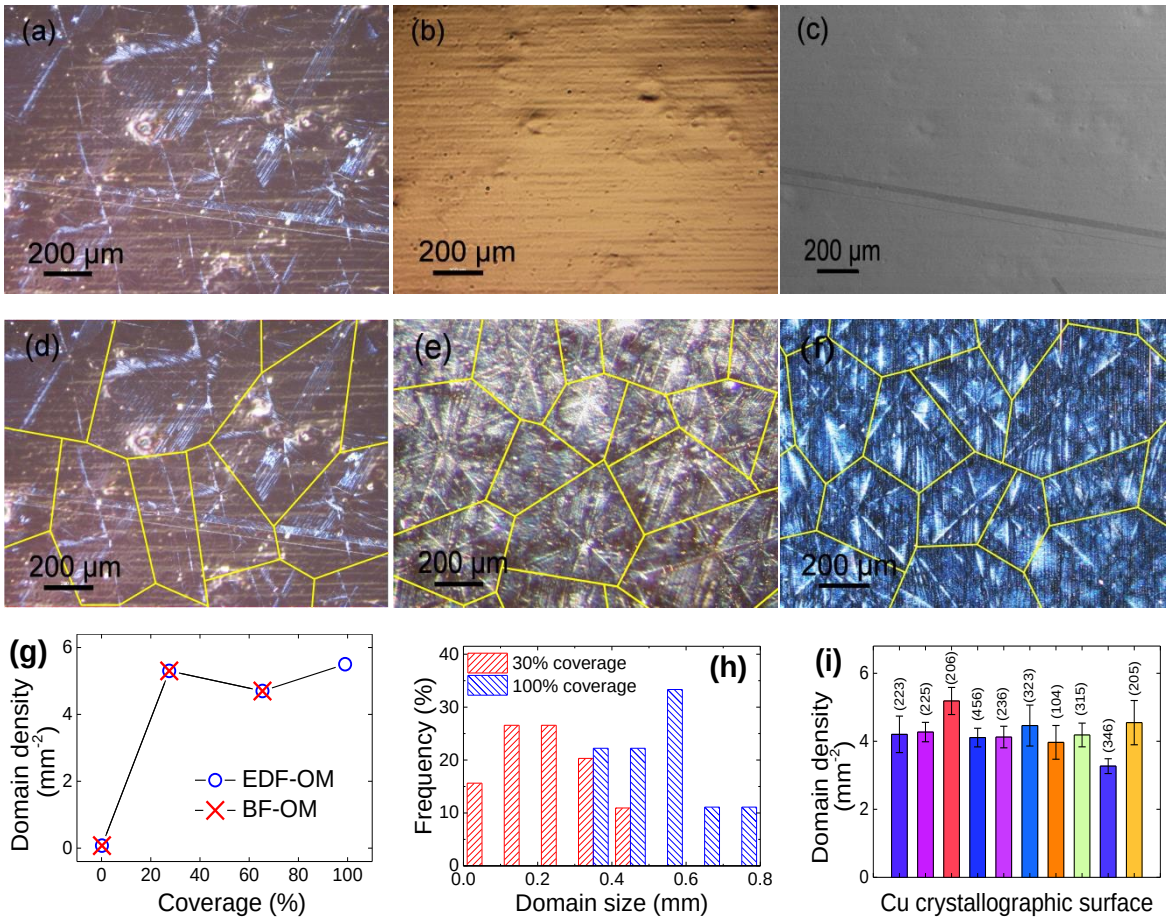

Fig. 4 (a) EDF-OM, (b) BF-OM and (c) SEM images of a typical continuous Gr/Cu. Only the EDF-OM can visualise the star-like ridge structures that are spatially corresponding to the graphene domains. (d-f) Outlining the graphene domains of continuous graphene films by the solid yellow polygons according to the fingerprint star-like ridge structures visualised by the EDF-OM. The solid polygons represent the approximate domain boundaries. The graphene films in (d-f) are obtained from crystallographically different Cu grains under the same CVD conditions. (g) Graphene domain density against coverage. CVD graphene with different coverage is grown by varying the carbon supply time. (h) Distributions of graphene domain sizes at ~100% coverage (determined by the EDF-OM) and ~30% coverage (determined by both the BF-OM and the EDF-OM). (i) Graphene domain density against Cu crystallographic orientations, which is counted from discontinuous Gr/Cu. The column colours are set equal to the EBSD mapping colours of the respective Cu surfaces.